

# Effects of the Growth Facet Shape of Self-Catalyzed GaAs Nanowires on the Zinc-Blende–Wurtzite Switching

Alexander A. Koryakin\* and Natalia V. Guruleva


Herein, the crystal phase switching between the cubic zinc-blende and hexagonal wurtzite phases in self-catalyzed GaAs nanowires (NWs) is theoretically studied, considering the dependence of the droplet contact angle on the position at the triple-phase line. This dependence is calculated for the droplets resting on the NW top facet, which has the shape of truncated hexagon. The nucleation of *c* and *h* islands, corresponding to the cubic and hexagonal crystal phases, at the triple-phase line and in the center of the catalyst–NW interface, is considered within the classical nucleation theory. As a result, the probability of *h*-island nucleation as a function of the average contact angle is obtained. It is found that the maximum of this probability shifts to the region of large contact angles when the length of narrow edges of the NW top facet decreases. Also, it is shown that the GaAs island nucleation at the triple-phase line occurs preferentially in the vicinity of the top facet corners.

## 1. Introduction

Semiconductor nanowires (NWs) grown by the vapor–liquid–solid (VLS) mechanism have a variety of potential applications in electronics, optoelectronics, photovoltaics, and sensorics due to their elongated shape, high crystalline quality, and the presence of quantum-size effects.<sup>[1–5]</sup> Particularly, III–V NWs are promising candidates for the fabrication of single-photon emitters,<sup>[2]</sup> high-quality multispectral photodetectors,<sup>[3]</sup> nanoantennas,<sup>[4]</sup> and high-performance transistors<sup>[5]</sup> integrated with silicon electronics. Self-catalyzed growth of III–V NW is usually performed by molecular beam epitaxy (MBE) or metal–organic chemical vapor deposition (MOCVD) on Si(111) substrates coated with a native or thermally grown oxide layer.<sup>[6,7]</sup> The growth technique involves the following stages. First, a lithographic patterning or thermal treatment of the substrate is applied to create pinholes in the oxide layer to seed gallium adatoms, which subsequently act as the VLS growth catalysts.

A. A. Koryakin  
Faculty of Physics  
St. Petersburg State University  
St. Petersburg 199034, Russia  
E-mail: koryakinaa@spbau.ru

N. V. Guruleva  
Laboratory of Epitaxial Nanotechnologies  
Alferov St. Petersburg Academic University  
St. Petersburg 194021, Russia

 The ORCID identification number(s) for the author(s) of this article can be found under <https://doi.org/10.1002/pssb.202300367>.

DOI: 10.1002/pssb.202300367

Second, after group V flux is turned on, the critical supersaturation is created in the droplets to start the VLS growth of GaAs inside the pinholes. Third, GaAs material fills the pinholes, and the NWs grow above the mask layer maintaining vertical orientation with respect to a (111) substrate. Note that the use of external catalysts (e.g., gold) for NW growth often causes the incorporation of the catalyst material into the growing crystal. This unwanted NW contamination is fully circumvented in the self-catalyzed VLS approach. Control over the shape and crystal phase of III–V NWs grown by the VLS mechanism is crucial for the design of devices with dedicated properties. Although the growth of III–V bulk semiconductors (except for nitrides) always occurs in the zinc-blende (ZB)

phase, both ZB and wurtzite (WZ) phases can be formed during the VLS growth of III–V NWs. The polytypism in III–V NWs obtained by the VLS method and the underlying crystal growth mechanisms have been studied for decades.<sup>[8–15]</sup> Let us briefly describe the main results of these studies. The preferred growth direction of III–V NWs is the  $[\bar{1}\bar{1}\bar{1}]$  direction, so that the NW top facet under the droplet is close-packed. There are two types of close-packing of atomic layers: cubic (ABCABC) and hexagonal (ABAB). Thus, geometrically, the difference between hexagonal and cubic packing is not so large. For example, if the misplacement occurs in the ABCABC sequence of the cubic lattice in the fifth layer (B layer is replaced by C layer) and then the further crystal growth occurs in the cubic phase, a twin (ABCACB) is formed. In this case, several layers (CAC) with hexagonal packing are formed. As a result, the crystal phase switching can occur due to a random misplacement of one of the layers. Since a single-monolayer forms by itself neither the ZB structure nor the WZ structure, it is convenient to use the following notation for the monolayer structure.<sup>[15]</sup> When a new monolayer is formed relative to two previous monolayers according to the ZB (WZ) stacking, A on BC (C on BC), it is denoted as c-monolayer (*h*-monolayer), i.e., cubic monolayer (hexagonal monolayer). The ZB and WZ structures containing stacking faults can also be described by this notation. The bulk WZ structure of GaAs at atmospheric pressure was found to have the energy about 20 meV pair<sup>−1</sup> higher than that of ZB and, therefore, the WZ phase is metastable.<sup>[16]</sup> Thus, the bulk WZ GaAs phase formation at the normal pressure can only be observed under exotic conditions.<sup>[17]</sup> At the same time, the phenomenon of polytypism and twinning processes is inherent to the nature of the VLS growth of nano- and microcrystals and was observed both in

GaAs NWs<sup>[15]</sup> and GaAs whiskers (microwires)<sup>[8]</sup> during their growth along the  $[111]/[\bar{1}\bar{1}\bar{1}]$  direction. Akiyama et al.<sup>[18]</sup> used the empirical potential approach to show that the WZ phase in III–V NWs is stable if the NW radii are small enough (about 5 nm for GaAs) due to the lower energy of the WZ NW side facets. The VLS growth of pure ZB GaAs NWs with such radii has been demonstrated later by Gil et al.<sup>[19]</sup> These results seem to be contradictive because, according to Akiyama's conclusions, one should observe a transient regime with the alternation of  $c$  and  $h$  layers for the NW radii of about 5 nm. However, it is known that kinetic factors play a crucial role in crystal growth with a specific shape and structure, and should also be considered for a realistic description of the ZB–WZ phase switching in III–V NWs.

Crystal growth occurs through the attachment of atoms to the step,<sup>[20]</sup> the source of which in the case of VLS NW growth is 2D nuclei (islands) at the catalyst–NW interface.<sup>[10,11,21]</sup> The position of the nucleus relative to the previous monolayers, i.e., its crystal orientation, determines the monolayer crystal structure. The kinetic approach of the classical nucleation theory is often used to study the VLS growth and to describe the related NW crystal structure.<sup>[11,12,22–25]</sup> This approach involves the consideration of the Gibbs formation energy for  $c$  and  $h$  nuclei and the use of the Zeldovich formula for the nucleation rate. Within this approach, it was shown<sup>[10,11]</sup> that the factors determining the crystal structure of the NW are as follows: 1) the chemical potential difference for species in liquid and solid phases per III–V pair, which depends on the element concentrations in the liquid phase and on the growth temperature. It is included as the bulk term in the Gibbs formation energy and is a priori smaller for the WZ nuclei. 2) The effective interphase energy per unit length of the island perimeter, which enters the surface energy term. For nucleation at the triple-phase line (at the edge of the NW top facet), the nucleation barrier strongly depends on the value of the droplet contact angle. The classical nucleation theory approach allowed one to establish that the nucleation barrier for  $h$  nuclei is lower than that for  $c$  nuclei within a range of the contact angles.<sup>[10]</sup> This is because the effective interphase energy of the part of the island perimeter in contact with the gas phase (the difference between the interphase energies of the liquid–vapor and solid–vapor interfaces) can be smaller than that for the solid–liquid interface. As a result, although the bulk term of the Gibbs formation energy is smaller for  $h$  island, there can be an energetic gain due to the surface energy term.

Most models based on the kinetic approach, with the exception of the model of ref. [26], use the assumption of cylindrical or cone-shaped NW geometry, which significantly simplifies theoretical calculations. In this case, the droplet having the minimum surface energy at a given volume has the shape of spherical cap, and the local contact angle is equal to the average contact angle. Since the effective interphase energy enters the exponent of the Zeldovich formula, the nucleation rate strongly depends on the variations of the contact angle. Note that this variation is equal to tens of degrees for the droplet resting on a hexagonal NW.<sup>[26]</sup> Moreover, the recent in-situ transmission electron microscopy (TEM) study of self-catalyzed GaAs NW growth<sup>[27]</sup> has shown that the WZ phase forms at the average contact angles in the range of  $\approx 100^\circ$ – $125^\circ$ , and that the NW crystal phase is sensitive to very small changes of the contact angle ( $\approx 5^\circ$ ) at the boundaries of this

range. These facts indicate that the consideration of the contact angle variation in hexagonal NW geometry is necessary for a refined description of the ZB–WZ switching.

In this article, we address the impact of the NW top facet geometry on the nucleation rate of  $c$  and  $h$  islands, depending on the value of the local contact angle. As in ref. [26], the droplet shape is obtained numerically by the gradient descent method using Surface Evolver software.<sup>[28]</sup> To calculate the island nucleation probability, we use the elements of the stochastic model<sup>[12]</sup> applied to the case of the Au-catalyzed GaAs NWs growth by MOCVD and further develop it to describe the NW growth by MBE. The expressions for the material fluxes from the vapor phase and for the chemical potential difference are determined according to the model of ref. [24]. The formula for the incorporation rate of III–V pairs into the critical island is taken from ref. [29]. We model the self-catalyzed GaAs NW growth considering different geometries of the NW top facet, in contrast to the model of ref. [26]. We show that the change of the NW top facet shape has an impact on the probability of  $h$  island nucleation, i.e., the crystal phase switching caused by the contact angle change.

## 2. Theoretical Model

### 2.1. Problem Definition

Let us consider layer-by-layer growth of self-catalyzed GaAs NWs in the  $[\bar{1}\bar{1}\bar{1}]$  direction due to the gallium and arsenic fluxes from the vapor phase (Figure 1). Since the catalyst droplet at the typical growth temperatures of 500–600 °C consists almost entirely of gallium atoms with a small arsenic content (less than  $\approx 2$  at%), we assume that the droplet volume is fixed and determined only by the number of gallium atoms. Modeling the monolayer formation is performed considering three components of the total arsenic flux in vapor phase:<sup>[24]</sup> the direct flux  $J_{AS}^{dir}$ , the re-evaporated flux  $J_{AS}^{re}$  and the desorption flux  $J_{AS}^{des}$ . As revealed by TEM and scanning electron microscopy techniques,<sup>[14,30–32]</sup> the GaAs NW side facets are usually  $\{\bar{1}\bar{1}2\}$  or  $\{\bar{1}\bar{1}0\}$  planes for ZB NW and  $\{\bar{1}\bar{1}00\}$  or  $\{\bar{1}\bar{1}20\}$  planes for WZ NW, so that NW has regular hexagonal cross section. It is natural to assume that the corners of the NW cross section are rounded due to thermal fluctuations and kinetic effects.<sup>[26]</sup> Therefore, as an approximation to the real NW geometry, we consider the NW top facet in the form of regular hexagon with truncated corners, bounded by the GaAs $\{\bar{1}\bar{1}2\}$  and GaAs $\{\bar{1}\bar{1}0\}$  planes (ZB segment formation) or by the GaAs $\{\bar{1}\bar{1}00\}$  and GaAs $\{\bar{1}\bar{1}20\}$  planes (WZ segment formation) as shown in Figure 1b. Also, it is assumed that the GaAs $\{\bar{1}\bar{1}2\}$  NW side facets are not stable and have the GaAs $\{\bar{1}\bar{1}2\}$  microfaceting with the GaAs $\{111\}$  and GaAs $\{\bar{1}\bar{1}\bar{1}\}$  facets. This corresponds to a more general case of the GaAs cross section obtained by the Wulff plot in ref. [33] where the following stable planes were considered:  $\{\bar{1}\bar{1}0\}$ ,  $\{100\}$ ,  $\{111\}$ , and  $\{\bar{1}\bar{1}\bar{1}\}$ . Note that the 12-corner GaAs cross section with the edges having comparable lengths was experimentally observed in ref. [34] for GaAs NW growth without catalyst. The NW top facet edges of different length (edge type 1 and edge type 2 in Figure 1b) bounded by the GaAs $\{\bar{1}\bar{1}2\}$  and GaAs $\{\bar{1}\bar{1}0\}$  planes in the ZB phase or by the GaAs $\{\bar{1}\bar{1}00\}$  and GaAs $\{\bar{1}\bar{1}20\}$

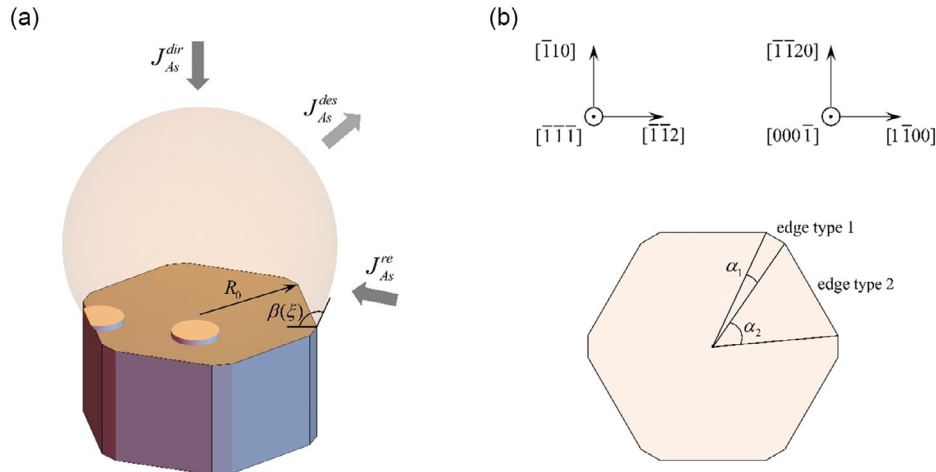


**Figure 1.** a) Schematic illustration of the apex of GaAs NW with the catalyst droplet. Two possible positions for the island nucleation are shown. b) The geometry of the NW top facet.

in the WZ phase are defined by the angles  $\alpha_1$  and  $\alpha_2$  (the sum of the angles equals  $60^\circ$ ).

The radius of the circumscribed circle around the NW top facet  $R_0$  defines the NW radius. The NW growth occurs due to mononucleation of islands located at the triple-phase line and islands that do not have contact with it (the center nucleation hereinafter) (Figure 1a). It is assumed that at the moment of nucleation of each monolayer, the NW top facet is atomically flat and there are no additional facets along its perimeter, as well as wetting of the NW sidewalls by the droplet. It should be noted that the faceting of the NW top facet in the case of NW growth in the  $[\bar{1}\bar{1}\bar{1}]$  direction observed in the experiments<sup>[14,27]</sup> at large droplet volumes is a periodic process, with the period approximately equal to the period of the monolayer formation. The edges of the NW top facet can dissolve during the monolayer growth; however, the crystal structure of the monolayer is determined at the moment of nucleation, so that the faceting does not directly affect the ZB–WZ switching.

To find the shape of the droplet resting on the NW top facet, we minimize the droplet surface area for a given volume. It is assumed that the droplet edges at the catalyst–NW interface are fixed, i.e., the droplet cannot detach from the triple-phase line. To prove this assumption, we verify that the local contact angle is greater than the critical angle  $\beta_c$ . We also note that numerical minimization of the droplet surface area requires consideration of the droplet surface as a continuous medium. As a result, the dependence of the local contact angle  $\beta$  (hereafter, the contact angle) on the coordinate  $\xi$  along the triple-phase line is found. This allows us to consider the effect of the variation of the contact angle on the nucleation rate of  $c$  and  $h$  islands at the triple-phase line. The contributions to the island nucleation probability from the nucleation at the edge type 1 and type 2 are calculated separately. The goal is to find and explain the dependence of the relative probability of  $h$  island nucleation on the droplet volume and, consequently, on the average contact angle considering different shapes of the NW top facet.

## 2.2. Island Shape

We consider a disk-shaped geometry of the islands for the center nucleation (Figure 1a). Indeed, let us assume that the ratios of the interphase energies corresponding to different orientations of the island edge (i.e., the  $\{111\}$ ,  $\{100\}$ , and  $\{110\}$  microfacets for  $c$  islands) equal to the ratios of the GaAs surface energies. Using the Wulff plot and reference data for GaAs surface energies,<sup>[33]</sup> we find that the islands should have the octagonal shape with different edge length ratio depending on the choice of the As-rich or Ga-rich condition. Given the errors in the surface energy calculations, the disk-shaped geometry of the island seems to be a reasonable approximation to the real shape. To describe the formation energy of a disk-shaped island, we introduce the effective interphase energy per unit length of the island perimeter denoting it as  $\sigma_{SL}$  (in  $\text{J m}^{-1}$ ).<sup>[20]</sup> For the nucleation at the triple-phase line, the equilibrium shape of the island is assumed in the form of circular segment. According to the Winterbottom construction used to find the equilibrium shape of the crystal in contact with the surface,<sup>[35]</sup> the island “sinks” in the solid–vapor interface so that the distance from the island center to the droplet surface  $h$  is determined as follows:  $h/R = (\sigma_{SV} - \sigma_{LV})/\sigma_{SL}$ , with  $\sigma_{SV}$  as the effective interphase energy of the solid–vapor interface;  $\sigma_{LV}$  as the effective interphase energy of the liquid–vapor interface per unit length (which is removed by the island formation); and  $R$  as the island radius.

## 2.3. Gibbs Energy of Island Formation

The Gibbs energy of the island formation in the form of a circular segment is given by<sup>[11,12]</sup>

$$\Delta G = -\frac{h_{\text{GaAs}}}{\Omega_{\text{GaAs}}} c_1 R^2 \Delta\mu + c_2 R \Sigma \quad (1)$$

where  $\Delta\mu$  is the chemical potential difference per GaAs pair in liquid and solid (this  $\Delta\mu$  is a function of the arsenic molar

fraction in the droplet  $N_{As}/N_{Ga}$ , where  $N_{As}$  and  $N_{Ga}$  are the number of arsenic and gallium atoms, and the growth temperature);  $h_{GaAs} = a_{GaAs}/3^{1/2}$  and  $\Omega_{GaAs} = a_{GaAs}^3/4$  are the GaAs monolayer height and volume per GaAs pair,  $a_{GaAs}$  is the GaAs lattice constant ( $h_{GaAs}$  and  $\Omega_{GaAs}$  are assumed to be the same for  $c$  and  $h$  islands);  $c_1$  and  $c_2$  are the geometrical factors that determine the island area  $c_1 R^2$  and perimeter  $c_2 R$  such that

$$\begin{aligned} c_1 &= \pi - \frac{1}{2} \left( 2 \arccos \frac{h}{R} - \sin \left( 2 \arccos \frac{h}{R} \right) \right), \\ c_2 &= 2 \left( \sqrt{1 - \frac{h^2}{R^2}} + \pi - \arccos \frac{h}{R} \right) \end{aligned} \quad (2)$$

The quantity  $\Sigma = (1 - x)\sigma_{SL} + x(\sigma_{SV} - \sigma_{LV})$  is the average interphase energy per unit length of the island perimeter;  $x$  is the fraction of the island perimeter in contact with the triple-phase line, determined by

$$x = \frac{\sqrt{1 - \frac{h^2}{R^2}}}{\sqrt{1 - \frac{h^2}{R^2}} + \pi - \arccos \frac{h}{R}} \quad (3)$$

The values of the interphase energies of the island perimeter are estimated from the known values of the corresponding surface energies. In particular,  $\sigma_{SL} \approx \gamma_{SL} h_{GaAs}$ . Following ref. [13], the interphase energy  $\sigma_{SV}$  is estimated as

$$\sigma_{SV} = \left( \frac{\gamma_{SV}}{\cos \varphi} - \gamma_{SL} \tan \varphi \right) h_{GaAs} \quad (4)$$

where  $\varphi$  is the tilt of the GaAs facet, which bounds the island edge at the solid–vapor interface (counted from the vertical such that the condition  $\varphi > 0$  corresponds to the narrowing facet);  $\gamma_{SV}$  and  $\gamma_{SL}$  are the surface energy of the solid–vapor interface, i.e., the droplet surface energy, and that of the solid–liquid interface. Thus, the effective interphase energy  $\sigma_{SL}$  is the average characteristics used to describe the formation energy of a unit length of the island perimeter in contact with the liquid phase. GaAs anisotropy is considered to determine the interphase energy  $\sigma_{SV}$  of the island edge in contact with vapor.

To calculate the interphase energy  $\sigma_{LV}$ , we use the approximate analytical dependence:<sup>[10,12,13]</sup>

$$\sigma_{LV} = \gamma_{LV} f(\beta, \varphi) h_{GaAs}, \quad f(\beta, \varphi) = \sin \beta + \cos \beta \tan \varphi \quad (5)$$

The function  $f(\beta, \varphi)$  determines the droplet surface area change due to the island formation. In the case of spherical droplet, this function yields a small error if the island perimeter in contact with vapor equals the perimeter of the NW top edge (this holds, e.g., for the full NW monolayer). By numerical calculation, we found that this formula can also be used for estimations in the case when the island size is much smaller than the NW top facet (Figure S4, Supporting Information). Using Equation (1), the nucleation barrier for the island in the form of circular segment is found in the same form as in ref. [12]

$$\Delta G(i_c) = \frac{c_2^2 \Omega_{GaAs} \Sigma^2}{4c_1 h_{GaAs} \Delta \mu} \quad (6)$$

where  $i_c = c_2^2 \Omega_{GaAs} \Sigma^2 / 4c_1 h_{GaAs} \Delta \mu^2$  is the critical island size. For disk-shaped island nucleation, we simply have  $h = R$  in Equation (1) and (6), giving  $c_1 = \pi$ ,  $c_2 = 2\pi$ ,  $x = 0$ , and  $\Sigma = \sigma_{SL}$ .

#### 2.4. Island Nucleation Probability and Monolayer Crystal Phase

The nucleation probability of at least one island on the NW top facet over the time period  $\Delta t = t_2 - t_1$  in the approximation of the Poisson distribution is given by<sup>[12]</sup>

$$P = 1 - \exp(-\langle N \rangle) \quad (7)$$

where  $\langle N \rangle$  is the average number of islands nucleated over the time period  $\Delta t$ :

$$\langle N \rangle = \int_{t_1}^{t_2} dt \int_A I dA \quad (8)$$

where  $I$  is the nucleation rate; and  $A$  is the area available for the island nucleation. Note that the Poisson distribution is often used for the theoretical description of NW growth.<sup>[12,25]</sup> The nucleation rate is determined according to the Zeldovich formula:<sup>[20]</sup>

$$I = n W^+ Z \exp(-\Delta G(i_c)/k_B T) \quad (9)$$

where  $W^+$  is the attachment rate of III–V pair to the critical island (in  $s^{-1}$ ),  $Z$  is the Zeldovich factor given by the formula:

$$Z = \frac{1}{c_2 \Sigma} \sqrt{\frac{c_1 h_{GaAs} \Delta \mu^3}{\pi \Omega_{GaAs} k_B T}} \quad (10)$$

$n = 4/(3^{1/2} a_{GaAs}^2)$  is the adsorption site density on the GaAs(111) surface,  $k_B$  is the Boltzmann constant, and  $T$  is the absolute temperature. The value of  $W^+$  is estimated according to the formula:  $W^+ \approx j^+$ , where the flux density of III–V pairs to the critical island  $j^+$  is determined by<sup>[29]</sup>

$$j^+ = \frac{\pi D_{As}}{\bar{\Omega} \ln(8 \pi R_c / h_{GaAs})} \quad (11)$$

where  $D_{As}$  is the diffusion coefficient of arsenic in gallium,  $\bar{\Omega}$  is the average volume per atom in the droplet (we assume that this volume equals the volume of gallium atom in liquid  $\Omega_{Ga}$ ), and  $R_c = c_2 \Omega_{GaAs} \Sigma / 2c_1 h_{GaAs} \Delta \mu$ . The island perimeter  $s$  for the disk-shaped island and for the island in the form of a circular segment equals  $2\pi R$  and  $2(\pi - \arccos(h/R))R$ . The area available for the center nucleation is the whole NW top facet area:

$$A = 3R_0^2 (\sin \alpha_1 + \sin \alpha_2) \quad (12)$$

For the island nucleation at the triple-phase line, the area available for nucleation is a thin strip along the NW top facet edge, whose width is determined by the critical island size and depends on the coordinate  $\xi$ . The elemental area  $dA$  equals

$$dA = q R_c \left( 1 + \frac{\sigma_{SV} - \sigma_{LV}}{\sigma_{SL}} \right) d\xi \quad (13)$$

where  $q$  is the symmetry factor ensuring that integration in Equation (8) is performed over a half of the NW top facet edge.

Thus, for the center nucleation and for nucleation at the triple-phase line, Equation (8) can be rewritten in the following forms:

$$\langle N^C \rangle = \int_{t_1}^{t_2} 3R_0^2 (\sin \alpha_1 + \sin \alpha_2) I dt \quad (14)$$

$$\langle N^{TPL} \rangle = \int_{t_1}^{t_2} dt \int_0^{\xi_{\max}} I q R_c \left( 1 + \frac{\sigma_{SV} - \sigma_{LV}}{\sigma_{SL}} \right) d\xi \quad (15)$$

In the model, we consider *c*- and *h*-island formation of different types at the triple-phase line depending on the angle  $\varphi$ . To calculate the nucleation probabilities of *c* and *h* islands,  $P_c$  and  $P_h$ , for the time  $\Delta t$  (Equation (7)), the value of  $\langle N \rangle$  is found according to

$$\langle N_c \rangle = \sum_{ij} \langle N_{c,ij}^{TPL} \rangle + \langle N_c^C \rangle \quad (16)$$

$$\langle N_h \rangle = \sum_{ij} \langle N_{h,ij}^{TPL} \rangle \quad (17)$$

where the index  $i = 1, 2$  denotes summation over different island types; and the index  $j$  refers to summation over different angles  $\varphi$ . In what follows, we consider nucleation of *c* islands at the edge types 1 and 2 (Figure 1b) having the following microfacets at the solid–liquid interface: GaAs{111} ( $\varphi = 19.5^\circ$ ,  $q = 6$ ), GaAs{ $\bar{1}\bar{1}\bar{1}$ } ( $\varphi = -19.5^\circ$ ,  $q = 6$ ), GaAs{100} ( $\varphi = 35.3^\circ$ ,  $q = 6$ ), and tilted GaAs{110} ( $\varphi = 54.7^\circ$ ,  $q = 6$ ) for the edge type 1; GaAs{110} ( $\varphi = 0^\circ$ ,  $q = 12$ ) for the edge type 2. Thus, the indexes  $ij$  in Equation (16) take the values of 11, 12, 13, 14, and 21, respectively. When *h* islands nucleate at the edge types 1 and 2, the following microfacets are allowed to form: GaAs{ $1\bar{1}00$ } ( $\varphi = 0^\circ$ ,  $q = 12$ ) and GaAs{ $11\bar{2}0$ } ( $\varphi = 0^\circ$ ,  $q = 12$ ), respectively. The indexes  $ij$  in Equation (17) take the values of 11 and 12. To calculate the average number of *c* islands, the contribution from the center nucleation,  $\langle N_c^C \rangle$ , is also included in Equation (16). The crystal phase of the growing monolayer is determined by the ratio of the nucleation probability of *h* islands over the sum of the nucleation probabilities of *h* and *c* islands<sup>[12]</sup>:  $P_h/(P_h + P_c)$ . This ratio for the small time period  $\Delta t \rightarrow 0$  is defined according to the simplified formula:

$$\lim_{\Delta t \rightarrow 0} \frac{P_h}{P_h + P_c} = \frac{\langle N_h \rangle}{\langle N_h \rangle + \langle N_c \rangle} = \frac{\sum_{ij} \langle N_{h,ij}^{TPL} \rangle}{\sum_{ij} \langle N_{h,ij}^{TPL} \rangle + \sum_{ij} \langle N_{c,ij}^{TPL} \rangle + \langle N_c^C \rangle} \quad (18)$$

## 2.5. Modeling Steps

Our computational algorithm consists of the following steps. 1) Set the growth parameters: temperature, arsenic flux, NW radius, NW top facet shape (angle  $\alpha_1$ ) and droplet volume. 2) Find the shape of the droplet resting on the nanofacet. 3) Calculate the arsenic molar fraction in the droplet as a function of the growth time. 4) Find the nucleation time  $\tau$  required to create supersaturation in the droplet. As in ref. [25], the estimation

of  $\tau$  is performed according to the following formula:  $\langle N \rangle = \ln(1/(1 - P))$ , where the probability  $P$  equals 0.5. The nucleation time is calculated for all types of islands at the triple-phase line ( $\tau = \tau_{h,ij}$  and  $\tau = \tau_{c,ij}$ ) and for the center nucleation ( $\tau_c$ ) using Equation (14) and (15), where we put  $t_1 = 0$  and  $t_2 = \tau$ . 5) Find the minimum nucleation time among islands of all types  $\tau_{\min} = \min\{\tau_{h,ij}, \tau_{c,ij}, \tau_c\}$ . 6) Calculate the relative probability of *h*-island nucleation by Equation (18) at the moment of time  $\tau_{\min}$ . To find the nucleation time self-consistently, the material balance equation for arsenic atoms in the droplet is considered in the form

$$\Delta N_{As} = (J_{As}^{\text{dir}} + J_{As}^{\text{re}} - J_{As}^{\text{des}}) \Delta t \quad (19)$$

where  $\Delta N_{As}$  is the change in the number of arsenic atoms over the time  $\Delta t$ ; the sum of the direct and re-evaporated arsenic fluxes is defined by the following equation:<sup>[24]</sup>  $J_{As}^{\text{dir}} + J_{As}^{\text{re}} = j_{As} S_{f,As}$ , where  $j_{As}$  is the effective arsenic flux density and  $S_{f,As}$  is the effective droplet cross-section area intersected by the direct arsenic flux. The desorption flux is defined by the following formula<sup>[24]</sup>:  $J_{As}^{\text{des}} = S_d k_{As} C_{As}^2$ , where  $S_d$  is the droplet surface area and  $k_{As}$  is the coefficient that characterizes desorption (see Supporting Information).

## 3. Results

### 3.1. Variation of Droplet Contact Angle

To determine the nucleation rate for islands located at the triple-phase line, it is necessary to calculate the values of the contact angle  $\beta$  as a function of the coordinate  $\xi$ . Figure 2a shows a typical result of the calculation for a fixed droplet volume and different shapes of the NW top facet. The details of the calculation obtained by Surface Evolver software can be found in Supporting Information. In Figure 2a, the coordinate  $\xi = 0$  corresponds to the middle of the edge type 2 and the maximum value of  $\xi$  corresponds to the middle of the edge type 1. It can be seen that the maximal values of  $\beta$  are at the middle of the edges and the minimal values are at the corner between the edge type 1 and type 2. It is important to note that the angle  $\beta$  changes faster in the vicinity of the corner between the edges, so that a wide range of angles is always observed in this region. As the angle  $\alpha_1$  decreases at a fixed droplet volume  $V_d$ , the average contact angle increases slightly due to the increase of the angle  $\beta$  at the wide edge (Figure S3, Supporting Information), but, simultaneously, the values of  $\beta$  at the narrow edge decrease. As a result, the range of existing contact angles increases. The presence of the narrow edges at the NW top facet causes the creation of favorable conditions at the triple-phase line for nucleation of islands having the angle  $\varphi$  from a wide range of values. At small droplet volumes, the calculated values of the droplet contact angle at the corners of the NW top facet can be less than the critical value  $\beta_c$ . In this case, we equate the values of the contact angle  $\beta$  to  $\beta_c$  (Figure 2b) in the calculation. This approximation is reasonable since, as shown later, the condition  $\beta < \beta_c$  is satisfied only for small intervals of  $\xi$ .

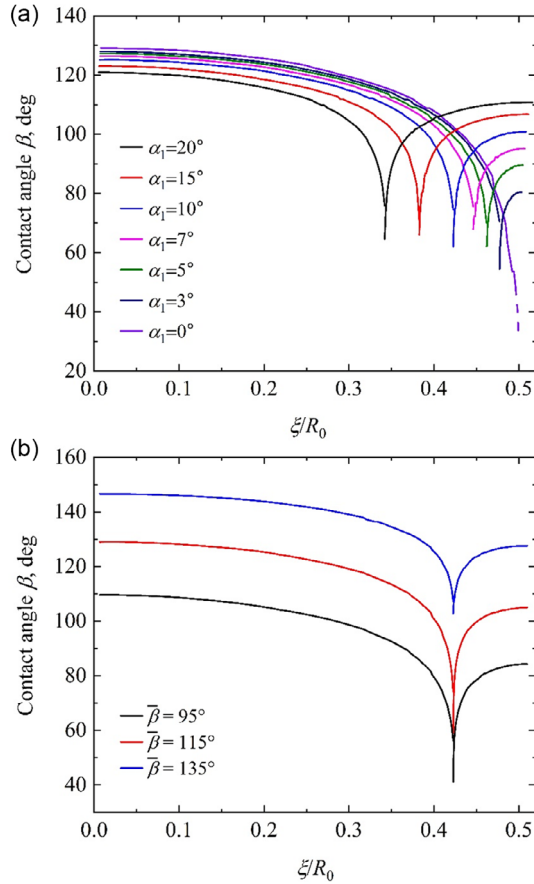


**Figure 2.** a) Calculated values of the contact angle versus the normalized coordinate along the edge of the NW top facet at a fixed droplet volume ( $V_d/R_0^3 = 3.6$ ) and different angles  $\alpha_1$  shown in the legend. b) Variation of the contact angle with the droplet volume.

### 3.2. Nucleation Rate at the Triple-Phase Line

Let us consider an example of calculation of the relative probability of  $h$ -island nucleation by Equation (18). The dependences of the nucleation rates (per unit length) on the position at the triple-phase line for the islands of different types and the relative probability of  $h$ -island nucleation are shown in **Figure 3** and **4**, respectively. Here, the growth temperature, arsenic flux, NW radius, and angle  $\alpha_1$  are fixed (the values of these quantities are given in the caption of Figure 3), but the droplet volume varies. The island nucleation rates at the triple-phase line were calculated using the integrand depending on the coordinate  $\xi$  in Equation (15) multiplied by  $R_0$ . The curves are plotted at the moments of time  $\tau_{\min}$  for each droplet volume. For comparison, the nucleation rate of  $c$  islands in the center of the catalyst–NW interface normalized to the growth facet perimeter is also shown. For this purpose, the integrand in Equation (14) is divided by the sum  $\xi_{1\max}/R_0 + \xi_{2\max}/R_0$ , where  $\xi_{1\max}$  and  $\xi_{2\max}$  is a half of the length of the edge type 1 and type 2, respectively. At small droplet volumes corresponding to the average droplet contact angles  $\bar{\beta}$  below  $105^\circ$  (Figure 3a,b), the nucleation rate of  $c$  islands is much higher than the nucleation rate of  $h$  islands. The nucleation of  $c$

islands with the tilted GaAs{110} microfacets in contact with vapor at the edge type 1 dominates due to their relatively low surface energy. This results in the negligibly small probability of  $h$ -island nucleation (see the values of the curve in Figure 4 at  $\alpha_1 = 10^\circ$  and  $\bar{\beta} < 105^\circ$ ). The contact angle corresponding to the maximum of the nucleation rate at  $\beta = 90^\circ - \varphi = 35.3^\circ$  is not observed, because, first, this value is smaller than the critical angle  $\beta_c$  and, second, the values of the minimum of the theoretical contact angles  $\beta_{\min}$  become larger than  $35.3^\circ$  with the increase of the droplet volume. The nucleation rates of islands of other types including the center nucleation are negligible in this case.

At the average contact angles in the range of  $\bar{\beta} \approx 113^\circ$ – $130^\circ$ , the total nucleation rates of  $c$  and  $h$  islands at the triple-phase line are comparable; however, the contribution of the center nucleation is still negligibly small. Figure 3c,d shows the typical dependencies of the nucleation rates on the coordinate  $\xi$  for a given range of the contact angles. Finally, after  $\bar{\beta} \approx 135^\circ$ , the center nucleation dominates (see Figure 3e,f). Note that the nucleation rate for the  $c$ -islands with the GaAs{100} microfacets is negligible in all cases.

Thus, we find that the island nucleation at the triple-phase line occurs preferentially in the regions close to the NW top facet corners (the minima of the  $\beta(\xi)$  dependencies shown in Figure 3 correspond to the corners), where favorable conditions exist for the nucleation of islands of different types (see Figure 3). When the droplet volume reaches large values, the NW growth occurs primarily due to the center nucleation. The average numbers of nucleation events per second calculated at the moment of time  $\tau_{\min}$  and obtained by integrating the nucleation rates along the triple-phase line are shown in Figure 3. Note that the estimation of  $\tau_{\min}$  using these maximal values gives a lower bound estimate. As a result, using Equation (18), we find the relative probability of  $h$ -island nucleation at three considered volumes: 0, 0.38, and 0.17 (compare with the curves in Figure 4). We also note that the ratio of  $h/R$  for the islands at the triple-phase line changes with the coordinate  $\xi$ , so that the island can “sink” deeper or shallower in the liquid–vapor interface. Obviously, the island edge length in contact with vapor reaches its maximum at the contact angle of  $\beta = 90^\circ - \varphi$ . The calculation shows that at this point the island is half “sunk” and  $h/R \approx 0$ . If this ratio becomes greater than 1, the island detaches from the triple-phase line. In this case, we assume the nucleation rate to be zero. Figure 3e,f shows the discontinuities in the curves for  $c$  islands due to this fact. The calculation performed for  $\beta_c = 55^\circ$  almost completely coincides with the calculation without considering  $\beta_c$  for the given contact angles  $\bar{\beta}$  and angles  $\alpha_1$ . This is due to the short range of the contact angles where  $\beta < \beta_c$ . The estimation of  $\beta_c$  was obtained by using the value of the critical angle  $\beta_c$  measured in the GaAs NW growth experiment after the droplet has detached from the triple-phase line and adopted a spherical shape.<sup>[27]</sup> The error of the calculation in Figure 4 was estimated by the error of the  $\beta(\xi)$  dependence (e.g.,  $\approx 0.03\%$  for the wide edge and  $\approx 0.1\%$  for the narrow edge at  $\alpha_1 = 10^\circ$ ). The absolute error for the probability in Figure 4 is typically of the order or less than 0.01 for all contact angles except for the regions of increasing probability where the typical error is of the order of 0.2. This is because the probability is determined by the competition

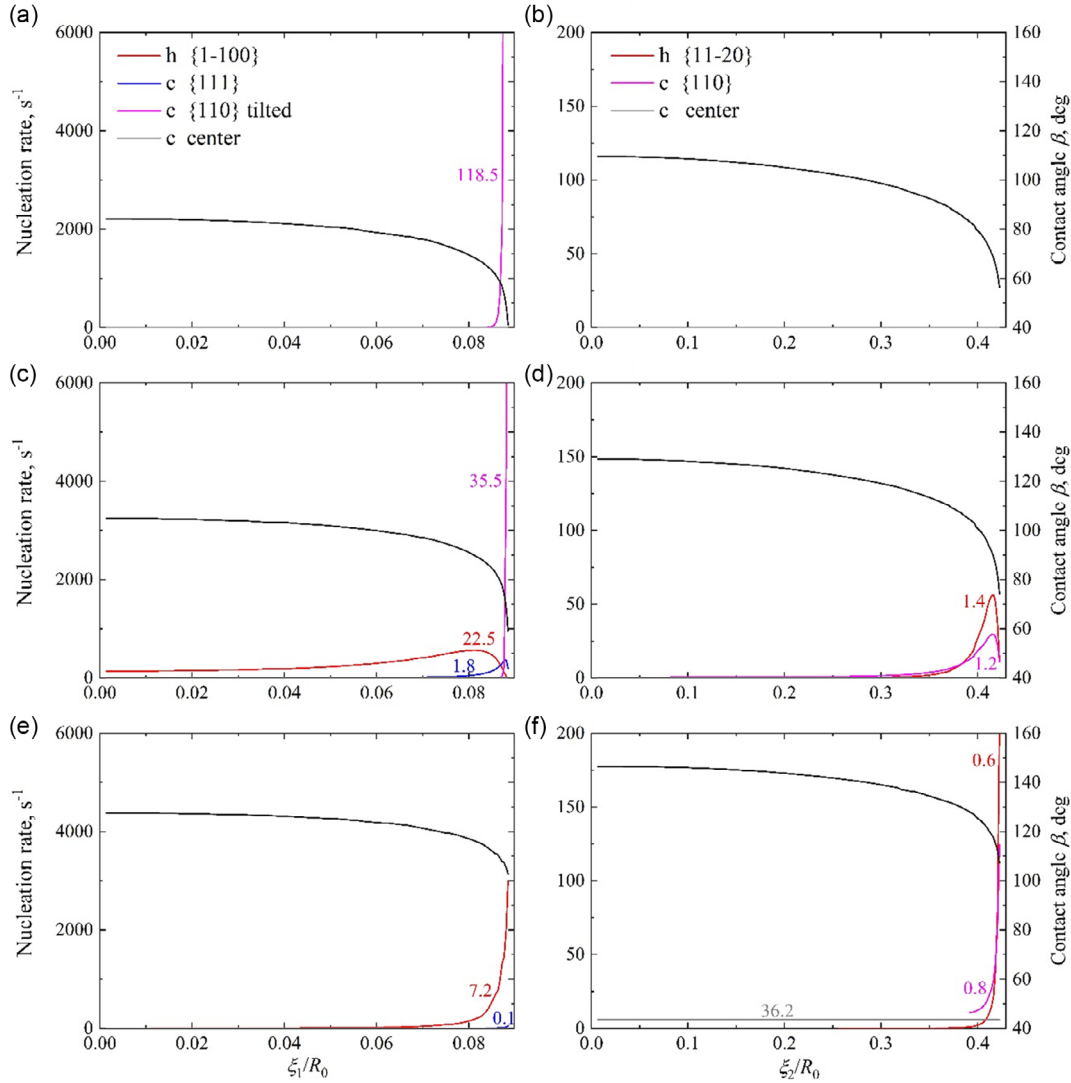


**Figure 3.** The island nucleation rate at the edge types 1 and 2 (left and right panels) at different values of the droplet volume corresponding to the average droplet contact angle of a,b) 95°, c,d) 115°, and e,f) 135°. The dependences of the contact angle on the coordinate are shown by black lines. It is seen that the maxima of the nucleation rates at the edge type 1 are at  $\beta = 90^\circ$  ( $h$  island),  $70.5^\circ$  ( $h$  island with the GaAs{111} microfacets), and at the edge type 2 are at  $\beta = 90^\circ$  ( $h$  island and  $c$  island). The maximum of the nucleation rate for  $c$  islands with tilted GaAs{110} microfacets ( $\beta = 35.3^\circ$ ) is not reached due to the cutoff of the  $\beta(\xi)$  function at  $\beta < \beta_c$ . The growth parameters are  $T = 500^\circ\text{C}$ ,  $j_{\text{As}} = 1 \times 10^{19} \text{ s}^{-1} \text{ m}^{-2}$ ,  $R_0 = 20 \text{ nm}$ , and  $\alpha_1 = 10^\circ$ . The numbers at the curves indicate the integrated values of the nucleation rates (in  $\text{s}^{-1}$ ). Note the different scale of the axis for the nucleation rate.

between  $c$  islands with tilted GaAs{110} microfacets and  $h$  islands in this region. The nucleation rate of the former has a sharp maximum at small angles, where the error is maximum. The calculations were performed using the values of the surface energies obtained in refs. [33,36,37] for the estimation of  $\gamma_{\text{SV}}$  and  $\gamma_{\text{SL}}$ . The values of the model parameters are given in Table S1, Supporting Information. It is also assumed that  $\Delta\mu = \Delta\mu_{\text{ZB}}$  for the  $c$ -island formation and  $\Delta\mu = \Delta\mu_{\text{ZB}} - \psi$  for the  $h$ -island formation, where  $\Delta\mu_{\text{ZB}}$  is the chemical potential difference between the ZB GaAs phase relative to the liquid Ga–As phase calculated by the Redlich–Kister polynomial equations as described by Glas,<sup>[24]</sup> and  $\psi$  is the difference in the cohesive energy between WZ and ZB phases.<sup>[12]</sup>

### 3.3. Dependence of the Relative Probability of $h$ -Island Nucleation on the NW Facet Shape

The relative probabilities of  $h$ -island nucleation calculated by our model are shown in Figure 4. It is seen that the curves shift to the right with the decrease of  $\alpha_1$ . At large values of  $\alpha_1$ , when the lengths of the edge type 1 and type 2 are comparable, the dependence changes slightly with the decrease of  $\alpha_1$ . However, if  $\alpha_1$  is smaller than  $10^\circ$ , the rate at which it changes with the variation of  $\alpha_1$  increases. For instance, the decrease of  $\alpha_1$  from  $10^\circ$  to  $5^\circ$  causes the shift of the maximum by about  $6^\circ$ , while the decrease of  $\alpha_1$  from  $30^\circ$  to  $20^\circ$  results in the shift by only  $2^\circ$ . The observed shift is due to the decrease of the minimum of the  $\beta(\xi)$

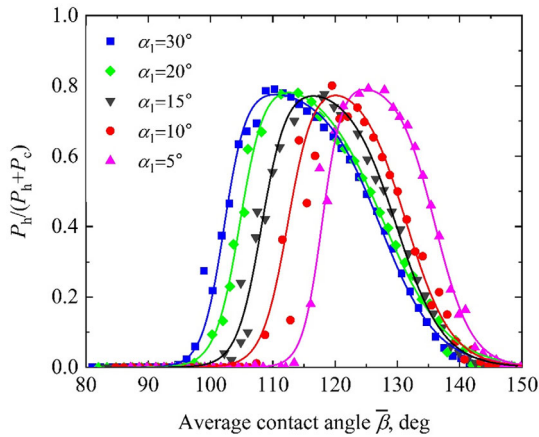


**Figure 4.** Dependence of the relative probability of *h*-island nucleation on the average contact angle. The calculations were performed at the following values of the model parameters:  $T = 500\text{ °C}$ ,  $j_{As} = 1 \times 10^{19}\text{ s}^{-1}\text{ m}^{-2}$ , and  $R_0 = 20\text{ nm}$ . The lines are a guide for the eye.

dependence with the decrease of  $\alpha_1$ . Indeed, the minimum of  $\beta(\xi)$  does not change significantly if  $\alpha_1$  is larger than  $10^\circ$ ; however, there is a sharp decrease in its value when  $\alpha_1$  tends to  $0^\circ$ . Thus, the droplet is stretched laterally more at the corners of the NW top facet, and the narrower thin edges (the smaller values of  $\alpha_1$ ), the greater the stretching. As a result, at the triplet phase line in the vicinity of the narrow edges, the values of contact angles “delay” as the droplet volume increases. This leads to the shift in the dependence of the relative probability of *h*-island nucleation with decreasing  $\alpha_1$ .

### 3.4. Effects of the NW Radius and Growth Temperature

In agreement with the previous theoretical investigations,<sup>[18,38,39]</sup> we found that the decrease of the NW radius causes the increase of the relative probability of *h*-island nucleation (Figure 5a). It is seen that the positions of the lower and upper WZ/ZB boundary change by  $4^\circ\text{--}6^\circ$  with the variation of the NW radius. Hereafter, we define the WZ/ZB boundary by the condition that the relative probability of *h*-island nucleation is 0.5. Within the model, we explain this fact by the increase of the arsenic content in the droplet (e.g., by 30% when the NW radius decreases from 50 to 10 nm). As shown in ref. [10], the difference in the value of  $\Delta\mu$  for *c* and *h* islands decreases with increasing the molar fraction of arsenic in the droplet at a fixed temperature. As a result, the nucleation barrier for *h* islands becomes smaller than for *c* islands due to the lower interphase energy of the solid–vapor interface  $\sigma_{SV}$  for *h* islands. The exception is the case of small radii ( $<5\text{ nm}$ ), where an increase in the arsenic desorption flux due to size effects leads to a decrease in the arsenic molar fraction.<sup>[24,29]</sup> We find that the relative decrease of the *c*-island nucleation probability for the center nucleation with the decrease of NW radii also affects the dependence shown in Figure 5a although to a lesser extent. Figure 5b shows that the growth temperature decrease causes the increase in the relative probability of *h*-island nucleation. Note that in this case the positions of the

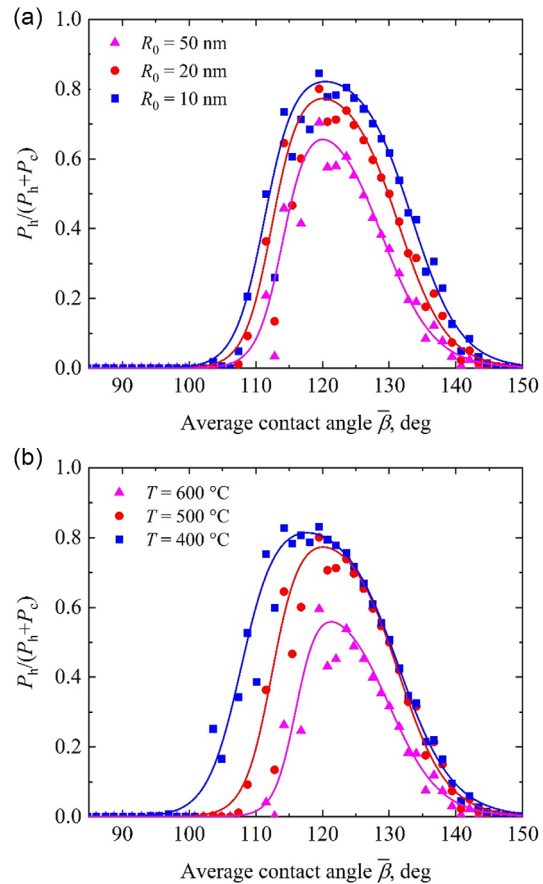


**Figure 5.** Variation of the relative probability of *h*-island nucleation with the change of a) the NW radius and b) the growth temperature. The model parameters, except for the NW radius in (a) or the growth temperature in (b), are the same as in Figure 4,  $\alpha_1 = 10^\circ$ .

WZ/ZB boundaries change by  $5^\circ\text{--}10^\circ$ . This is due to the fact that, despite the decrease of arsenic solubility in the gallium droplet, the chemical potential difference  $\Delta\mu_{ZB}$  increases and, therefore, the relative height of the nucleation barrier for *h* islands decreases. Also, Figure 5a,b shows that the maximum of the curves is almost independent of the NW radius; however, its position changes slowly with the temperature.

In addition, we find that the dependence of nucleation probabilities on the arsenic flux is very weak (not shown); however, an increase of the arsenic flux causes an increase in the NW growth rate. This is explained by the fact that for intensive nucleation it is necessary to lower the nucleation barrier to a certain threshold value, which depends only on the thermodynamic factors. As a result, when the flux changes, the island nucleation occurs approximately at the same values of nucleation barrier<sup>[12]</sup> and arsenic molar fraction. The typical values of the NW growth rate and the arsenic molar fraction at the arsenic flux of  $j_{As} = 1 \times 10^{19}\text{ s}^{-1}\text{ m}^{-2}$  and  $R_0 = 20\text{ nm}$  are of the order of  $2\text{ nm s}^{-1}$  and 0.1 at% for  $T = 500\text{ °C}$  and  $0.7\text{ nm s}^{-1}$  and 0.6 at% for  $T = 600\text{ °C}$ .



## 4. Discussion

In this section, we discuss the validation of the obtained results. First, we compare the theoretical results with the experimental data on the VLS growth of GaAs NWs. Panciera et al.<sup>[27]</sup> found that the WZ phase in self-catalyzed GaAs NWs forms at the average contact angle within the range of 100°–125° at  $T = 420$  °C and  $R_0 \approx 15$  nm. Using the value of  $\alpha_1 = 15^\circ$ , we obtain a satisfactory agreement in the positions of the lower and upper WZ/ZB boundary for the droplet contact angles, 106° and 128°, respectively. The maximum of the theoretical dependence of the relative probability of *h*-island nucleation (about 0.8) is slightly lower than the values corresponding to the formation of almost pure WZ phase observed in the experiment. Note that the angle  $\alpha_1$  defining the size of the narrow edges of NW top facet is the only fitting parameter in this calculation. Panciera et al.<sup>[27]</sup> observed no clear dependence of the positions of the lower and upper WZ/ZB boundary on the NW radius and growth temperature. The observed variation by 7°–10° in the values of these boundaries (at variable temperature) is explained within the model by the change of the growth facet shape. Also, an important result of our modeling is that the island nucleation at the triple-phase line predominantly occurs at the corners of the NW top facet. Due to the small size of the critical nucleus (a few III–V pairs), it is challenging to experimentally find the nucleation site on the NW top facet by modern TEM equipment.<sup>[30]</sup> Although the results of the investigation of Au-catalyzed growth of GaAs NWs having WZ structure<sup>[30]</sup> provide an indirect confirmation of our model. The smallest island (occupying about 10% of the top facet area) was formed at the triple-phase line in contact with the facet corner. Similar result was obtained in ref. [40], but the island was in contact with two corners of the NW top facet. The experimental data<sup>[14,27]</sup> show that the ZB phase formation at large droplet volumes is accompanied by the periodic dissolution of the growth facet edge. It was found that the onset of this process coincides with the moment of crystal phase switching from WZ to ZB. Jacobsson et al.<sup>[14]</sup> argued that the dissolution even a part of the top facet edge creates new preferential sites for *c*-island nucleation with a high nucleation rate. Thus, there is the second critical angle  $\beta'_c$  (not to be confused with  $\beta_c$ ) at which the top facet edge becomes truncated. Using our model and the experimental values of the upper WZ/ZB boundary ( $\beta \approx 125^\circ$ ),<sup>[14,27]</sup> we estimate the value of  $\beta'_c \approx 139^\circ$  reached in the middle of the wide edges of the growth facet. This corresponds to the droplet contact angle of  $\approx 49^\circ$  (for  $\alpha_1 = 5^\circ$ – $15^\circ$ ) with the vertical NW sidewalls, which is in agreement with the data on the equilibrium contact angle of Ga droplet on the GaAs surfaces.<sup>[27,41]</sup> Accounting for this effect in the model would lead to a sharper ZB–WZ transition at large droplet volumes compared to that shown in Figure 4 and 5 due to the presence of a new term in the *c*-island nucleation probability and/or the disappearance of nucleation sites at the triple-phase line. Moreover, in this case, the shape of the dependencies of *h*-island nucleation probability would vary slightly with the change of  $\alpha_1$  after reaching  $\bar{\beta} \approx 125^\circ$ .

Let us now discuss the various sources of errors in the theoretical approach used in the calculations. Since there is usually some range of the surface energy values obtained by

density-functional theory methods, we compare the results of the calculations using the reference data<sup>[33,36,39]</sup> for defining  $\gamma_{SV}$ . We find that due to variation of the surface energy by about 5%, the magnitude of the maximum of the relative probability of *h*-island nucleation changes by about 20%, and its position by about 4°. Also, the increase in the value of  $\gamma_{SL}$  by 30% yields the increase in the height of the maximum of the dependence by 13% and causes the shift of its position by 10° to the right. We vary the value of  $\gamma_{SL}$  in a larger range because in the literature there are only few references to the studies where this quantity was estimated.<sup>[37]</sup> In addition, the results of the simulation depend strongly on the set of island types nucleating at the triple-phase line. For example, if we excluded from consideration *c* islands with the tilted GaAs{110} microfacets, it would lead to a significant increase in the relative probability of *h*-island nucleation at small contact angles and to the broadening of the region of WZ phase formation by more than a factor of 2 (the interphase energies  $\gamma_{SV}$  and  $\gamma_{SL}$  were the same). However, at large average contact angles, when the nucleation rate of islands of the given types was negligibly small, the dependence would be completely the same. The NW side facets GaAs{110} were chosen for comparison with the experiment.<sup>[27]</sup> It was found that the modeling the NW growth with the GaAs{ $\bar{1}\bar{1}2$ } side facets yields results very similar to those for the GaAs{110} side facet formation (not shown).

It is important to emphasize that the developed model for the island nucleation on the NW top facet, as the models,<sup>[11,12,22,24]</sup> is essentially macroscopic. Indeed, the physical quantities included in the Gibbs energy of island formation (Equation (1)) ( $\sigma_{SV}$ ,  $\sigma_{SL}$ ,  $\sigma_{LV}$ , and  $\Delta\mu$ ) are estimated from the data for bulk materials. Also, the additional assumption is used to estimate the change in the droplet surface area during island nucleation (Equation (5)), namely, we consider the surface of the gallium droplet near the island as a continuous medium. At the same time, there may be atomic wetting mechanisms that cannot be described within the framework of classical macroscopic concepts.<sup>[35]</sup> Therefore, we conclude that to calculate the probabilities of island nucleation with a higher accuracy, it is necessary to calculate the energy barriers of nucleation based on microscopic consideration, for example, by using various ab initio methods. In addition, the role of the intermediate state of atoms in the droplet near the catalyst–NW interface with “partial ordering” remains poorly understood,<sup>[42]</sup> as well as other collective mechanisms of nucleation. Although these issues are beyond the scope of the present article, this does not diminish the significance of the developed model, which allows us to investigate the general qualitative laws of the ZB–WZ switching in NWs.

## 5. Conclusion

In summary, a model of self-catalyzed GaAs NW growth was developed which considers the NW top facet in the form of a truncated hexagon. The dependences of the droplet contact angles on the position at the triple-phase line were obtained for droplets resting on the NW top facet of different shapes. Using these dependences, the nucleation rates of *c* and *h* islands, corresponding to the cubic ZB and hexagonal WZ crystal phases, at the triple-phase line and in the center of the catalyst–NW

interface, were calculated. The nucleation of islands with different tilt angle of microfacets at the solid–liquid boundary was considered. As a result, the dependences of the relative probability of *h*-island nucleation on the average contact angle were obtained for the case of NW growth with different top facet shape. We found that the maximum of this dependence shifts to larger contact angles when the length of narrow edges of the NW top facet decreases. It was shown that the island nucleation at the triple-phase line occurs preferentially in the vicinity of the NW top facet corners due to the presence of a wide range of contact angles. Although at large contact angles, the nucleation of *c* islands in the center dominates. Our findings on the preferential sites for island nucleation are consistent with the experimental observations. Also, the theoretical predictions for the width and position of the interval of contact angles at which the WZ phase forms are in agreement with the existing experimental data. The obtained results are important for further development of the theory of polytypism in III–V NWs grown by the VLS mechanism.

## Supporting Information

Supporting Information is available from the Wiley Online Library or from the author.

## Acknowledgements

The authors gratefully acknowledge financial support of St. Petersburg State University under the research grant no. 94033852.

## Conflict of Interest

The authors declare no conflict of interest.

## Data Availability Statement

The data that support the findings of this study are available from the corresponding author upon reasonable request.

## Keywords

III–V semiconductors, molecular-beam epitaxies, nanowires, vapor–liquid–solid growth

Received: August 13, 2023

Revised: January 12, 2024

Published online:

- [1] E. Barrigón, M. Heurlin, Z. Bi, B. Monemar, L. Samuelson, *Chem. Rev.* **2019**, *119*, 9170.
- [2] P. Yu, Z. Li, T. Wu, Y.-T. Wang, X. Tong, C.-F. Li, Z. Wang, S.-H. Wei, Y. Zhang, H. Liu, L. Fu, Y. Zhang, J. Wu, H. H. Tan, C. Jagadish, Z. M. Wang, *ACS Nano* **2019**, *13*, 13492.
- [3] Z. Li, S. Trendafilov, F. Zhang, M. S. Allen, J. W. Allen, S. U. Dev, W. Pan, Y. Yu, Q. Gao, X. Yuan, I. Yang, Y. Zhu, A. Bhat, S. X. Peng, W. Lei, H. H. Tan, C. Jagadish, L. Fu, *Nano Lett.* **2021**, *21*, 7388.
- [4] O. Sorias, A. Kelrich, R. Gladstone, D. Ritter, M. Orenstein, *Nano Lett.* **2017**, *17*, 6011.
- [5] O.-P. Kilpi, J. Svensson, J. Wu, A. R. Persson, R. Wallenberg, E. Lind, L.-E. Wernersson, *Nano Lett.* **2017**, *17*, 6006.
- [6] M. R. Ramdani, J. C. Harmand, F. Glas, G. Patriarche, L. Travers, *Cryst. Growth Des.* **2013**, *13*, 91.
- [7] S. Ermez, E. J. Jones, S. C. Crawford, S. Gradečak, *Cryst. Growth Des.* **2015**, *15*, 2768.
- [8] J. J. Nickl, W. Just, *J. Cryst. Growth* **1971**, *11*, 11.
- [9] E. I. Givargizov, *Krist. Tech.* **1975**, *10*, 473.
- [10] F. Glas, J.-C. Harmand, G. Patriarche, *Phys. Rev. Lett.* **2007**, *99*, 146101.
- [11] V. G. Dubrovskii, N. V. Sibirev, J. C. Harmand, F. Glas, *Phys. Rev. B* **2008**, *78*, 235301.
- [12] E. K. Mårtensson, S. Lehmann, K. A. Dick, J. Johansson, *Nano Lett.* **2019**, *19*, 1197.
- [13] V. G. Dubrovskii, *Cryst. Growth Des.* **2017**, *17*, 2544.
- [14] D. Jacobsson, F. Panciera, J. Tersoff, M. C. Reuter, S. Lehmann, S. Hofmann, K. A. Dick, F. M. Ross, *Nature* **2016**, *531*, 317.
- [15] J. Johansson, J. Bolinsson, M. Ek, P. Caroff, K. A. Dick, *ACS Nano* **2012**, *6*, 6142.
- [16] C.-Y. Yeh, Z. W. Lu, S. Froyen, A. Zunger, *Phys. Rev. B* **1992**, *46*, 10086.
- [17] M. I. McMahon, R. J. Nelmes, *Phys. Rev. Lett.* **2005**, *95*, 215505.
- [18] T. Akiyama, K. Sano, K. Nakamura, T. Ito, *Jpn. J. Appl. Phys.* **2006**, *45*, L275.
- [19] E. Gil, V. G. Dubrovskii, G. Avit, Y. André, C. Leroux, K. Lekhal, J. Grecenkov, A. Trassoudaine, D. Castelluci, G. Monier, R. M. Ramdani, C. Robert-Goumet, L. Bideux, J. C. Harmand, F. Glas, *Nano Lett.* **2014**, *14*, 3938.
- [20] I. V. Markov, *Crystal Growth for Beginners*, World Scientific, Singapore **2003**.
- [21] F. Glas, F. Panciera, J.-C. Harmand, *Phys. Status Solidi Rapid Res. Lett.* **2022**, *16*, 2100647.
- [22] V. G. Dubrovskii, N. V. Sibirev, *Phys. Rev. E* **2004**, *70*, 031604.
- [23] J. Johansson, L. S. Karlsson, C. Patrik, T. Svensson, T. Mårtensson, B. A. Wacaser, K. Deppert, L. Samuelson, W. Seifert, *Nat. Mater.* **2006**, *5*, 574.
- [24] F. Glas, M. R. Ramdani, G. Patriarche, J.-C. Harmand, *Phys. Rev. B* **2013**, *88*, 195304.
- [25] Y. Y. Hervieu, *J. Cryst. Growth* **2021**, *568–569*, 126187.
- [26] P. Krogstrup, S. Curiotto, E. Johnson, M. Aagesen, J. Nygård, D. Chatain, *Phys. Rev. Lett.* **2011**, *106*, 125505.
- [27] F. Panciera, Z. Baraissov, G. Patriarche, V. G. Dubrovskii, F. Glas, L. Travers, U. Mirsaidov, J.-C. Harmand, *Nano Lett.* **2020**, *20*, 1669.
- [28] K. A. Brakke, *Exp. Math.* **1992**, *1*, 141.
- [29] A. A. Koryakin, S. A. Kukushkin, *Phys. Status Solidi Basic Res.* **2021**, *258*, 2000604.
- [30] J.-C. Harmand, G. Patriarche, F. Glas, F. Panciera, I. Florea, J.-L. Maurice, L. Travers, Y. Ollivier, *Phys. Rev. Lett.* **2018**, *121*, 166101.
- [31] B. A. Wacaser, K. Deppert, L. S. Karlsson, L. Samuelson, W. Seifert, *J. Cryst. Growth* **2006**, *287*, 504.
- [32] D. Wolf, R. Hübner, T. Niermann, S. Sturm, P. Prete, N. Lovregine, B. Büchner, A. Lubk, *Nano Lett.* **2018**, *18*, 4777.
- [33] N. Moll, A. Kley, E. Pehlke, M. Scheffler, *Phys. Rev. B* **1996**, *54*, 8844.
- [34] E. Chereau, V. G. Dubrovskii, G. Grégoire, G. Avit, P. Staudinger, H. Schmid, C. Bougerol, P.-M. Coulon, P. A. Shields, A. Trassoudaine, E. Gil, R. R. LaPierre, Y. André, *Cryst. Growth Des.* **2023**, *23*, 4401.
- [35] W. D. Kaplan, D. Chatain, P. Wynblatt, W. C. Carter, *J. Mater. Sci.* **2013**, *48*, 5681.
- [36] M. Rosini, R. Magri, *ACS Nano* **2010**, *4*, 6021.
- [37] S. Sakong, Y. A. Du, P. Kratzer, *Phys. Rev. B* **2013**, *88*, 155309.

- [38] E. K. Mårtensson, S. Lehmann, K. A. Dick, J. Johansson, *Cryst. Growth Des.* **2020**, *20*, 5373.
- [39] V. Pankoke, P. Kratzer, S. Sakong, *Phys. Rev. B* **2011**, *84*, 075455.
- [40] M. Marnauza, M. Tornberg, E. K. Mårtensson, D. Jacobsson, K. A. Dick, *Nanoscale Horizons* **2023**, *8*, 291.
- [41] C. Chatillon, D. Chatain, *J. Cryst. Growth* **1995**, *151*, 91.
- [42] M. Zamani, G. Imbalzano, N. Tappy, D. T. L. Alexander, S. Martí-Sánchez, L. Ghisalberti, Q. M. Ramasse, M. Friedl, G. Tütüncüoğlu, L. Francaviglia, S. Bienvenue, C. Hébert, J. Arbiol, M. Ceriotti, A. Fontcuberta i Morral, *Adv. Mater.* **2020**, *32*, 2001030.